TRR
JOURNAL OF THE TRANSPORTATION RESEARCH BOARD

Research Article

Transportation Research Record
1–11

DOI: 10.1177/0361198119827530
journals.sagepub.com/home/trr
SAGE

Applicability of Modified University of Illinois at Urbana–Champaign Model for Unbound Aggregate Material with Different Water Content

Tianshu Lin[1], Tatsuya Ishikawa[2], and Bin Luo[1]

Abstract

This paper proposes a modified University of Illinois at Urbana–Champaign (UIUC) model to predict permanent deformation behavior of unbound aggregate materials. Most existing models relate permanent deformation to resilient properties, whereas the UIUC model treats shear strength as a critical factor in permanent deformation behavior. Three types of test, monotonic shearing test, cyclic axial loading test, and cyclic axial and shear loading test, were conducted by multi-ring shear apparatus on two kinds of parallel grading aggregate materials, natural crusher-run and recycled crusher-run obtained from demolished concrete structure. Test results demonstrate that shear strength is the core factor in permanent deformation behavior, compared with resilient properties, and principal stress axis rotation (PSAR) greatly increases the permanent deformation. By considering the effect of PSAR on permanent deformation, a new parameter, $(R_s)_{ave}$, is added to the conventional UIUC model to modify it. Regression analysis results verify that the modified UIUC model has good applicability for predicting permanent deformation of aggregates with different water contents and stress states, and with and without PSAR. The modified UIUC model builds a relation between test results with and without PSAR. A simple framework is also proposed for predicting permanent deformation in flexible pavement structures based on the modified UIUC model.

Permanent deformation of base layers caused by traffic wheel loads is one of the primary pavement failure mechanisms, because the main function of the base layer is to provide structural support to the top layer of the pavement. Permanent deformation of unbound aggregate materials is influenced by many factors, such as particle size distribution, density, water content, the strength of materials, loading history, the stress level, the loading numbers, principal stress axis rotation (PSAR), and so forth.

Many predictive models have been proposed based on more or fewer factors listed above. The Mechanistic-Empirical Pavement Design Guide (MEPDG) model (*1*), which is based on the Tseng-Lytton model (*2*), relates the permanent strain to the resilient modulus. On the other hand, the NCHRP Project 4-23 pointed out that shear strength but not resilient modulus is one of the most significant mechanical properties influencing pavement performance (*3*). Then, the K-T model (*4*) and UIUC model (*5*) use shear strength to construct a predictive model. As a result, the UIUC model shows high accuracy on permanent strain prediction.

However, the applicability of the UIUC model to materials with different moisture contents has not been verified. In addition, all these models are based on results from the repeated loading triaxial test, which has a constant confining stress, and do not consider the effect of PSAR, which is always encountered under in-situ conditions and has a great effect on permanent deformation (*6–9*).

The objective of this study is to implement all these limitations mentioned above. To simulate the in-situ stress state in the pavement, Ishikawa et al. (*10*) developed a multi-ring shear apparatus for laboratory element tests, which could apply cyclic axial load and shear stress. This paper utilizes multi-ring shear test results obtained by Inam (*11*) to check which one of resilient modulus or shear strength is the more significant factor in permanent deformation. Then, the UIUC model is modified by

[1]Graduate School of Engineering, Hokkaido University, Sapporo, Japan
[2]Faculty of Public Policy, Hokkaido University, Sapporo, Japan

Corresponding Author:
Address correspondence to Tianshu Lin: ts_lin@eis.hokudai.ac.jp

considering the effect of PSAR on permanent strain. The modified UIUC model is validated at various moisture contents and stress states.

Existing Models for Rut Depth Prediction

The unbound materials permanent deformation model developed by Tseng and Lytton (*2*) is shown by

$$\varepsilon_p = \varepsilon_0 e^{-\left(\frac{\rho}{N}\right)^{\beta}} \tag{1}$$

where

ε_p is the permanent strain;

N is the number of loading cycles;

ε_0 is the maximum permanent strain because when N tends to infinity, $\varepsilon_p = \varepsilon_0$;

ρ is the scale factor;

β is the shape factor; and

ε_0, β, and ρ are unknown parameters which are determined by regression analysis.

However, the stress effect is ignored in this model. Therefore, the value of the three parameters variate with different stress levels and the relationships between them are established based on a statistical analysis. The regression models normally have relatively low R^2 values.

Equation 2 is the MEPDG model (*1*), which converts the plastic strain measured from the laboratory to the field condition. A threshold value of rut depth is used to determine the life of the pavement structure.

$$\varepsilon_p(N) = \beta_1 \left(\frac{\varepsilon_0}{\varepsilon_r}\right) e^{-\left(\frac{\rho}{N}\right)^{\beta}} \varepsilon_v \tag{2}$$

where

$\varepsilon_p(N)$ is the permanent strain for the layer/sub-layer;

N is the number of traffic repetitions;

ε_0, β, and ρ are material properties;

ε_r is the resilient strain imposed in a laboratory test to obtain material properties ε_0, β, and ρ;

ε_v is the average vertical resilient strain in the layer/sub-layer, which is calculated by a multilayer elastic pavement response model; and

β_1 is the calibration factor for the unbound granular and subgrade materials.

As normal, a larger stress state will lead to a larger permanent deformation, and it can be seen from Equation 2 that the MEPDG model evaluates this effect of stress level indirectly by considering the average vertical resilient strain in the layer/sublayer.

El-Basyouny and Witczak (*1*; Appendix GG) developed a final model modification that could be used in the design guide as shown in Equations 2–6. The strain ratio, $\varepsilon_p/\varepsilon_v$, in the equation is a function of the layer modulus for different traffic levels. Assuming values for $\varepsilon_p/\varepsilon_v$ at different loading numbers, $N = 1$ and $N = 10^9$, to calculate the a_1, b_1, a_9, and b_9 values, $a_1 = 0.15$, $b_1 = 0$, $a_9 = 20$, and $b_9 = 0$ are "universal" constants obtained from national calibrations.

$$\frac{\varepsilon_0}{\varepsilon_r} = \frac{e^{\rho^{\beta}} * a_1 * E^{b_1} + e^{\left(\frac{\rho}{10^9}\right)^{\beta}} * a_9 * E^{b_9}}{2} = \frac{e^{\rho^{\beta}} * 0.15 + e^{\left(\frac{\rho}{10^9}\right)^{\beta}} * 20}{2} \tag{3}$$

$$\log\beta = -0.61119 - 0.017638 W_c \tag{4}$$

$$\rho = 10^9 \left(\frac{C_0}{1-\left(10^9\right)^{\beta}}\right)^{\frac{1}{\beta}} = 10^9 \left(\frac{-4.89285}{1-\left(10^9\right)^{\beta}}\right)^{\frac{1}{\beta}} \tag{5}$$

$$C_0 = \ln\left(\frac{a_1 * E^{b_1}}{a_9 * E^{b_9}}\right) = -4.89285 \tag{6}$$

where E is resilient modulus and W_c is water content.

Chow et al. (*5*) used MEPDG to predict the permanent strain of four materials. The results show that predictive permanent strain in MEPDG has a strong relationship with resilient modulus, which is also obvious from Equation 2. Moreover, the water content also greatly influences the permanent strain in two ways: first, the water content decides the value of β as shown in Equation 4; second, the resilient modulus is also affected by the water content.

Equation 7 shows the K-T model proposed by Korikiala-Tanttu.

$$\varepsilon_p = CN^b \frac{R}{1-R} \tag{7}$$

where

ε_p is the permanent vertical strain;

C is the permanent strain in the first loading cycle;

N is the number of loading cycles;

b is the shear ratio parameter depending on the material (Equation 8); and

R is the shear failure ratio (Equation 9).

$$b = d\left(\frac{q}{q_f}\right) + c' \tag{8}$$

$$R = \frac{q}{q_f} = \frac{\sigma_1 - \sigma_3}{q_0 + Mp} \tag{9}$$

$$q_0 = c\frac{6\cos\phi}{3-\sin\phi} \tag{10}$$

$$M = \frac{6\sin\phi}{3-\sin\phi} \tag{11}$$

where

q is deviator stress;

q_f is the deviator stress in failure;

q_0 is the deviator stress when $p\tilde{A}\text{¢}\S$ equals zero;

c is the cohesion;

ϕ is the friction angle;

M is the slope of the failure line in p'-q space in the triaxial test; and

c' and d are material parameters.

The UIUC model is based on the phenomenological model (*12*) as shown in Equation 12. Then, deviator stress and shear stress ratio (SSR) are added onto it, and the UIUC model is shown in Equations 13 to 17.

$$\varepsilon_p(N) = AN^B \tag{12}$$

$$\varepsilon_p(N) = AN^B {\sigma_d}^C \left(\frac{\tau_f}{\tau_{\max}}\right)^D \tag{13}$$

$$\text{SSR} = \frac{\tau_f}{\tau_{\max}} \tag{14}$$

$$\tau_f = \sqrt{\left(\frac{\sigma_d}{2}\right)^2 - \left[\sigma_f - \left(\sigma_3 + \frac{\sigma_d}{2}\right)\right]^2} \tag{15}$$

$$\sigma_f = \frac{2\sigma_3(1 + \tan^2\phi) + \sigma_d(1 + \tan^2\phi) - \sqrt{{\sigma_d}^2\tan^2\phi(1 + \tan^2\phi)}}{2(1 + \tan^2\phi)} \tag{16}$$

$$\tau_{\max} = c + \sigma_f \tan\phi \tag{17}$$

where

$\varepsilon_p(N)$ is the permanent strain corresponding to N-load applications;

σ_d is applied deviator stress;

τ_f is mobilized shearing resistance acting on the failure plane;

σ_f is normal stress acting on the failure plane;

$\tau_{\max}$ is available shear strength obtained through Mohr-Coulomb failure criteria; and

A to D are regression parameters.

According to the author, the applied deviator stress term is enough to capture the effects of stress levels with constant confining pressure and the effect of confining pressure is indirectly reflected in the calculation for mobilized shearing resistance. The effect of shear strength on permanent deformation is considered by incorporating the SSR term. In Chow et al. (*13*), the effects of moisture content on permanent deformation accumulation are not considered because their tests were conducted at optimum moisture content—maximum dry density conditions. Therefore, the accuracy of the UIUC model for predicting permanent deformation of aggregates with different moisture contents is not verified and the effect of PSAR on permanent deformation is also ignored.

Materials and Testing Program

Materials used in this research include natural crusher-run with 40 mm maximum particle size (C-40) and recycled crusher-run which is obtained from demolished concrete structure and has 40 mm maximum particle size (C-40). As the width of the specimen is 60 mm and the minimum diameter of the mold sizes to fabricate specimens should be equal to or greater than five times the maximum particle size (*14*), the maximum particle size selected in this research was 9.5 mm. After screening out particles larger than 9.5 mm, test materials are named as C-9.5 (natural crusher-run) and RC-9.5 (recycled crusher-run) in this paper. As fine particles may enter the small gaps of the rings of the multi-ring shear apparatus, materials were washed inside the 0.075 mm sieve to remove the fine particles. Moreover, these two materials are parallel grading materials. More property details about these materials, such as grain size distribution and soil water characteristic curve (SWCC), are shown by Inam (*11*).

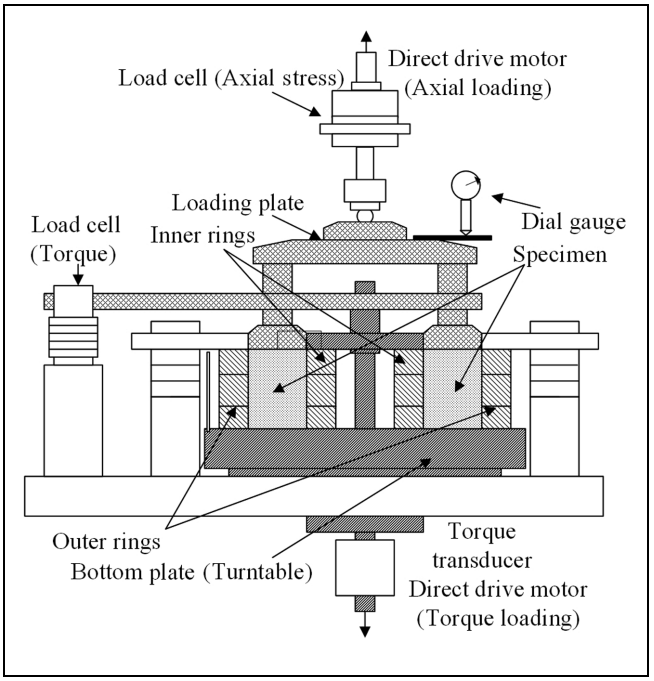

Figure 1. Multi-ring shear apparatus (after Ishikawa et al. *15*).

Ishikawa et al. (*10*) developed a multi-ring shear apparatus for laboratory element tests, which could apply cyclic axial loading and shear stress simultaneously. The width of the specimen is 60 mm and the height is 60 mm. Shear strain and axial strain is calculated through transducers. The schematic diagram of the multi-ring shear apparatus is shown in Figure 1.

Inam performed a series of monotonic and cyclic loading tests (*11*, *16*). The degree of saturation (S_r) of the specimen was selected as S_r = 19%, 33%, and 48% based on the field data obtained from Tomakomai, Japan. An oven-dried sample was also selected to compare the results with those of the unsaturated specimen. A dry density of 1.581 to 1.583 g/cm^3 was selected for the multi-ring shear tests. The stress states for the multi-ring

Table 1. Experimental Conditions for Multi-Ring Shear Tests

Test material	Degree of saturation, S_r (%)	Dry density after consolidation, ρ_{dc} (g/cm^3)	Monotonic shearing tests		FL tests		ML tests	
			Constant axial stress, σ_a (kPa)	Shear strain rate, (%/min)	Maximum axial stress, $(\sigma_a)_{max}$ (kPa)	Maximum shear stress, $(\tau_{a\theta})_{max}$ (kPa)	Maximum axial stress, $(\sigma_a)_{max}$ (kPa)	Maximum shear stress, $(\tau_{a\theta})_{max}$ (kPa)
C-9.5	Oven dried	1.58	114.2	0.1	114.2	0	114.2	30/15
	19	1.58	114.2	0.1	114.2	0	114.2	30/15
	33	1.58	114.2	0.1	114.2	0	114.2	30/15
	48	1.58	114.2	0.1	114.2	0	114.2	30/15
RC-9.5	Oven dried	1.47	114.2	0.1	114.2	0	114.2	30
	19	1.47	114.2	0.1	114.2	0	114.2	30
	33	1.47	114.2	0.1	114.2	0	114.2	30
	48	1.47	114.2	0.1	114.2	0	114.2	30

shear tests were determined based on a stress analysis of a Japanese paved road model using the General Analysis Multilayered Elastic Systems approach (GAMES, *17*). The multi-ring shear apparatus simulates the field loading conditions by applying the axial load and the shear load in a sinusoidal waveform. The loading frequency in this study was 0.02 Hz because of the limitation of the apparatus.

Three types of tests were performed—monotonic shearing test, cyclic axial loading test, and cyclic axial and shear loading test. In monotonic shearing tests, keeping axial stress constant, shear stress increased monotonically at the rate of a shear strain of $\gamma_{a\theta} = 0.1\%$/min until the shear strain reached 3%. In the cyclic axial loading test, axial load was applied in the sinusoidal waveform to the specimen, which is similar to a repeated loading triaxial test without rotation of the principal stress axis. In this research, the cyclic axial tests are referred to as fixed-place loading tests (FL tests). In the cyclic axial and shear loading test, the axial load and the shear load, both in the sinusoidal waveform, are cyclically applied to the specimen. The shear load is cyclically applied for bidirectional loading, similar to two-way traffic on pavement, by changing the phase angle of 180° for every succeeding loading cycle. This test is considered as a moving-wheel loading test (ML test), in which the rotation of the principal stress axis occurs similarly to in-situ traffic loading conditions. The numbers of loading cycles of FL tests and ML tests were both 400. Several tests under identical conditions were performed and the coefficient of variation (CoV) was 8.89%, which could validate the accuracy of the test method and apparatus. Based on this accuracy, each type of experiment was performed once and the test results are treated as accurate and precise. The experimental conditions for the multi-ring shear tests performed in this research are summarized in Table 1.

Dependency of Permanent Strain on Shear Strength

A higher resilient modulus leads to a smaller average vertical resilient strain (ε_v) and finally a lower permanent strain in MEPDG as shown in Equation 2. In addition, the water content just affects the curve shape of permanent strain with number of loading cycles but will not affect the ratio of permanent strain to resilient strain as shown in Equation 2. However, from the multi-ring shear test results, these dependencies are not always true. Figure 2*a* indicates the resilient and permanent strain in the last loading cycle of the FL test and ML test. The solid and dashed lines connect the scatter by the sequence of permanent strain of C-9.5 and RC-9.5 respectively. C-9.5 shows smaller permanent deformation than that of RC-9.5 when the water content and applied stress are the same, which illustrates that these two materials have different mechanical properties, though they share similar grain size distribution. In Figure 2*a*, the tendency of permanent strain to increase with increasing resilient strain only exists in RC-9.5 in the FL test and all other test results did not show this tendency. Moreover, the effect of water content on permanent strain is significant. For example, oven-dried and 19% degree of saturation RC-9.5 in the ML test show similar resilient strain around 0.05, but their permanent strain varies a lot. Moreover, the dependency of permanent strain on test material can also be observed. Oven-dried C-9.5 and RC-9.5 in the FL test share the same water content and similar resilient strain, but the permanent strain is different. In addition, permanent strain in the ML test is three to four times greater than it is in the FL test, which illustrates the great effect of PSAR on permanent strain, and this effect should be considered. As a result, it is obvious that the dependency between resilient modulus and permanent strain varies a lot and a prediction of permanent strain based on the MEPDG model may not be accurate.

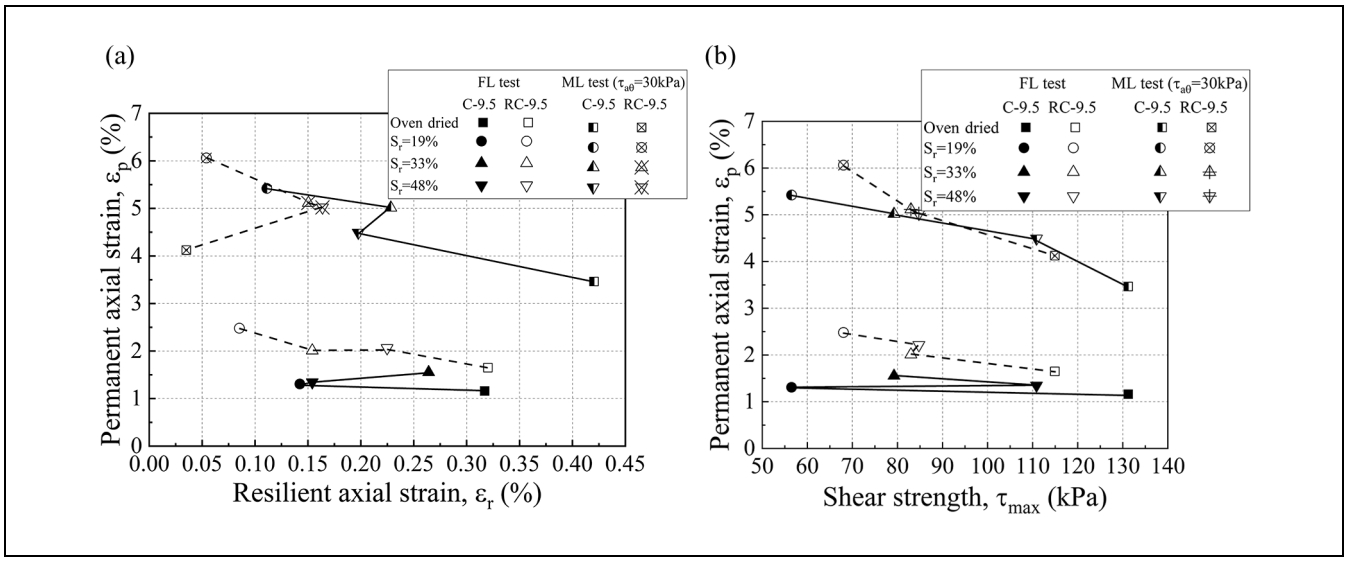

Figure 2. Relations between permanent axial strain and (*a*) resilient axial strain and (*b*) shear strength.

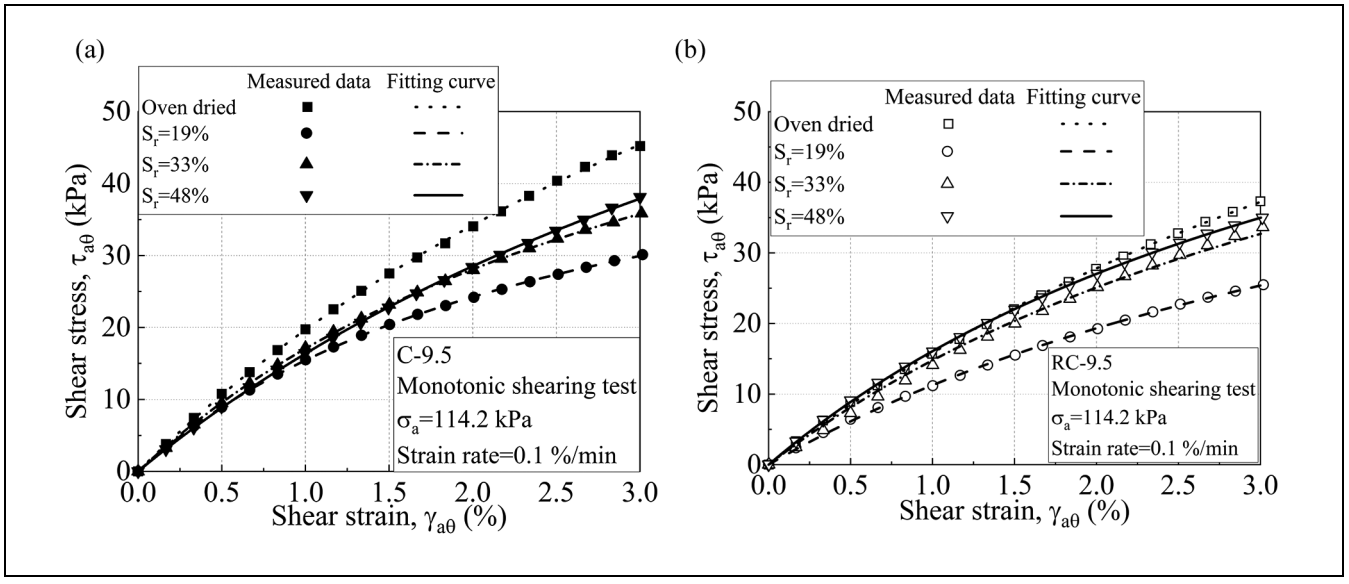

Figure 3. Shear stress-strain curve in monotonic shearing test for (*a*) C-95 and (*b*) RC-95.

On the other hand, the shear strength has a strong effect on permanent deformation in the UIUC model as shown in Equation 13. In this study, the shear strength of the C-9.5 and RC-9.5 is estimated by applying the Duncan-Chang model (*18*), shown in Equations 18 and 19, to test the results of the monotonic shearing test.

$$\sigma_1 - \sigma_3 = \frac{\varepsilon}{a + b\varepsilon} \tag{18}$$

$$(\sigma_1 - \sigma_3)_{\text{ult}} = \frac{1}{b} \tag{19}$$

where

a and b are material constants;

the reciprocal of a is the initial tangential Young's modulus; and

the reciprocal of b is the failure value of stress difference.

For the monotonic shearing test performed by multi-ring shear apparatus, the above equations change to the following forms. The regression analysis result is shown in Figure 3 and Table 2.

$$\tau_{a\theta} = \frac{\gamma_{a\theta}}{a + b\gamma_{a\theta}} \tag{20}$$

$$\tau_{\max} = (\tau_{a\theta})_{\text{ult}} = \frac{1}{b} \tag{21}$$

Table 2. Regression Analysis Results with Duncan-Chang Model

Materials	Degree of saturation, S_r (%)	a	b	R^2	τ_{max} (kPa)
C-9.5	Oven dried	0.04322	0.00762	0.999	131.23
	19	0.04711	0.01770	0.999	56.50
	33	0.04599	0.01262	0.999	79.24
	48	0.05210	0.00902	0.999	110.86
RC-9.5	Oven dried	0.05449	0.00870	0.999	114.94
	19	0.07411	0.01470	0.999	68.03
	33	0.05562	0.01205	0.998	82.99
	48	0.05040	0.01180	0.999	84.75

Note: a = material constants; b = material constants; R^2 = coefficient of determination; τ_{max} = shear strength.

Table 3. Results of Regression Analysis through Modified UIUC Model

Test materials	Test types	A	B	C	D	E	R^2	RMSE
C-9.5	FL	0.55174	0.12753	1.31838	0.78153	NA	0.951	0.059
	ML (15kPa)	0.85226	0.11425	1.11295	1.09863	2.72659	0.959	0.148
	ML (30kPa)	0.57746	0.15822	1.73123	0.67476	3.02101	0.900	0.428
RC-9.5	FL	0.99402	0.09052	0.68875	0.86966	NA	0.932	0.097
	ML (30kPa)	1.60651	0.13132	0.88051	0.95224	0.29498	0.980	0.162

Note: A to E = regression parameters; R^2 = coefficient of determination; RMSE = root mean square error; NA = not available.

Figure 2*b* shows the relation between estimated shear strength and permanent axial strain of the last loading cycle. The solid and dashed line connect the scatter by the sequence of permanent strain of C-9.5 and RC-9.5 respectively. There is a significant tendency for higher shear strength to lead to smaller permanent axial strain regardless of the type of materials, with the sole exception of C-9.5 with S_r = 19% and RC-9.5 with S_r = 33% in the FL test, which may be because of some experimental error happening during the tests. Comparing Figure 2, *a* and *b*, it is reasonable to conclude that the dependency between shear strength and permanent strain is more significant than the dependency between resilient strain and permanent strain, which is the reason to choose the UIUC model but not the MEPDG model to predict the permanent strain.

Proposal and Application of Modified UIUC Model

To capture the effect of PSAR on permanent deformation, a parameter, $(R_s)_{ave}$, proposed by Ishikawa et al. (*15*, *19*) is used. $(R_s)_{ave}$ means the average ratio of axial strain between specimens with and without PSAR. In addition, $(R_s)_{ave}$ could be roughly approximated by

$$(R_s)_{ave} = \exp\left(A\frac{(\tau_{a\theta})_{max}}{(\sigma_a)_{max}}\right) \quad (22)$$

where

$(\sigma_a)_{max}$ is the maximum applied axial stress;
$(\tau_{a\theta})_{max}$ is the maximum applied shear stress; and
A is a material constant.

As the definition of stress is not the same in triaxial compression tests and multi-ring shear tests, the SSR is transferred to modified SSR ($SSR = [\tau_{a\theta}]_{max}/[\tau_{max}]$). However, this ratio cannot be used in the FL test because applied shear stress is zero and modified SSR also equals zero. Moreover, the maximum shear stress, $(\tau_{a\theta})_{max}$, already exists in $(R_s)_{ave}$. Based on the above reasons, the SSR is modified to

$$SSR = \frac{1}{\tau_{max}} \quad (23)$$

where τ_{max} is shear strength.

Adding modified SSR and $(R_s)_{ave}$ to the UIUC model, the modified UIUC model for multi-ring shear tests (both ML test and FL test) is obtained as

$$\varepsilon_p(N) = AN^B(\sigma_a)_{max}{}^C\left(\frac{1}{\tau_{max}}\right)^D \exp\left(E\frac{(\tau_{a\theta})_{max}}{(\sigma_a)_{max}}\right) \quad (24)$$

Before applying this equation for predicting permanent deformation of unbound aggregate materials, normalization should be finished. A normalized equation is shown by

$$\varepsilon_p(N) = AN^B\left(\frac{(\sigma_a)_{\max}}{p_a}\right)^C\left(\frac{p_a}{\tau_{\max}}\right)^D \exp\left(E\frac{(\tau_{a\theta})_{\max}}{(\sigma_a)_{\max}}\right) \quad (25)$$

where p_a means the atmospheric pressure, equal to 101 kPa in this study.

All necessary input parameters, stress state, and shear strength, for regression analysis with the modified UIUC model are shown in Tables 1 and 2. Notice that, during regression analysis, the real stress condition detected by transducer, not the proposed stress condition, was used.

Regression analysis results with this model are shown in Table 3. The R^2 value is high enough to prove the applicability of the modified UIUC model. As a supplement to the R^2, the value of root mean square error (RMSE) is also calculated. The value of RMSE is also low enough to validate the accuracy of this model. Figures 4 and 5 compare the measured experimental data and the permanent deformation model predictions.

In Figure 4*a* and *b*, there are only three approximation lines, not four, as the curve of $S_r = 19\%$ is excluded. For materials with lowest shear strength, they should have the largest deformation. This phenomenon may be caused by experimental errors. For example, the suction cannot be controlled in this apparatus and the uniformity of water may not be ensured. Except for these two (C-9.5 with $S_r = 19\%$ in the FL test and the ML test with 15 kPa maximum shear stress), all other fitting curves through the modified UIUC model show good consistency with test results.

Moreover, if the newly added parameter, $(R_s)_{\text{ave}}$, could connect regression analysis results between the FL test and ML test, then it should also be capable of connecting regression analysis results between the repeated loading triaxial test and the ML test, because the FL test is similar to the repeated loading triaxial test. In other words, when test results obtained from laboratory test without PSAR are multiplied by this new parameter, they can be treated as test results with PSAR. A large quantity of test data obtained from a traditional repeated loading triaxial test could be closer to an in-situ condition.

To check the applicability of this newly added parameter, when conducting regression analysis for ML test results, the values of *A, B, C*, and *D* were fixed to the same value obtained from the FL regression analysis results. The results are shown in Figure 6 and Table 4.

Comparing Tables 3 and 4, the R^2 value decreases a little but is still higher than 0.9, except for the ML test (maximum shear stress of 30 kPa) of C-9.5. The small variance of RMSE value proves the reliability of this fixed-parameter model, though this value increases a little. This result illustrates the applicability of $(R_s)_{\text{ave}}$.

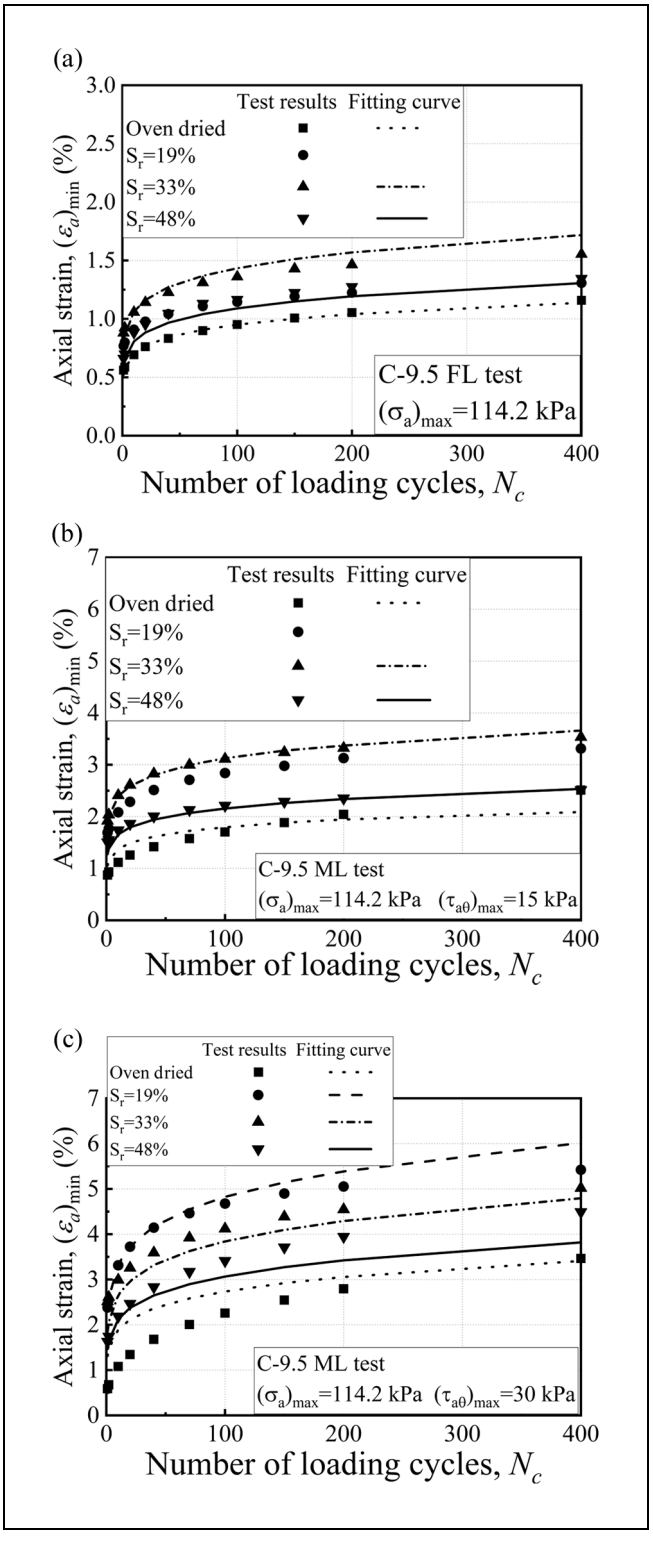

Figure 4. Estimation of permanent axial strain of C-9.5 for (*a*) FL test, (*b*) ML test ($[\tau_{a\theta}]$max = 15 kPa), and (*c*) ML test ($[\tau_{a\theta}]$max = 30 kPa).

As a result, the modified UIUC model displays good applicability to the test results of the multi-ring shear test.

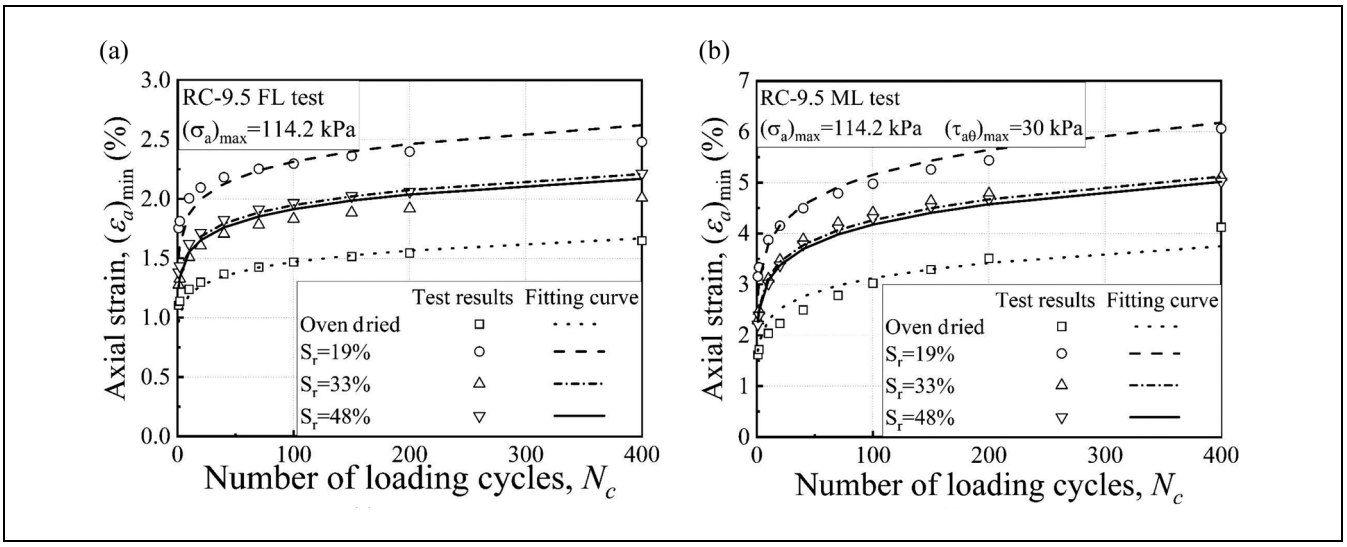

Figure 5. Estimation of the permanent axial strain of RC-9.5 for (*a*) FL test and (*b*) ML test.

Table 4. Results of Regression Analysis through Modified UIUC Model with Fixed Parameters

Test materials	Test types	*A*	*B*	*C*	*D*	*E*	R^2	RMSE
C-9.5	FL	0.55174	0.12753	1.31838	0.78153	NA	0.951	0.059
	ML (15kPa)	0.55174	0.12753	1.31838	0.78153	5.60922	0.910	0.213
	ML (30kPa)	0.55174	0.12753	1.31838	0.78153	3.77173	0.866	0.460
RC-9.5	FL	0.99402	0.09052	0.68875	0.86966	NA	0.932	0.097
	ML (30kPa)	0.99402	0.09052	0.68875	0.86966	2.91403	0.922	0.310

Note: *A* to *E* = regression parameters; R^2 = coefficient of determination; RMSE = root mean square error; NA = not available.

Moreover, all parameters have clear physical significance: parameter A represents the initial permanent strain; parameter B represents the development of permanent strain with the number of loading cycles; parameter C reflects the effect of applied axial stress on permanent strain; parameter D captures the effect of shear strength on permanent strength; and parameter E represents the effect of PSAR on permanent strain. For parameter E in particular, this value connects test results obtained from laboratory tests with and without PSAR. After calibration of these five parameter values, this new model could be used in engineering design.

Model Implementation for Predicting Rut Depth of Flexible Pavement

The first step for predicting rut depth of the base layer in flexible pavement structures through the modified UIUC model is determining the stress state in the base layer. In this research, the stress state in flexible pavement structure is determined by General Analysis of Multilayered Elastic Systems (GAMES, *17*). In this regard, a Japanese paved road model under standard design wheel loads is selected, as shown in Figure 7. The properties of the pavement layers, which include elastic coefficient E and Poisson's ratio v, the standard wheel load, the wheel diameter, and the distance between wheels, shown in Figure 7, are also indicated in the *Pavement Design Manual* for Japanese paved roads (*20*).

After obtaining the stress distributions in the base layer, the multilayered incremental approach is employed to compute the total rut depth. The following equation explains how the total rut depth of the base layer is computed using the modified UIUC model.

$$\delta_p(N) = \int_0^h AN^B \left(\frac{(\sigma_a)_{\max}(z)}{p_a}\right)^C \left(\frac{p_a}{\tau_{\max}}\right)^D \exp\left(E\frac{(\tau_{a\theta})_{\max}(z)}{(\sigma_a)_{\max}(z)}\right) dz \quad (26)$$

where

$\delta_p(N)$ is rut depth of base course;

h is total height of base course; and

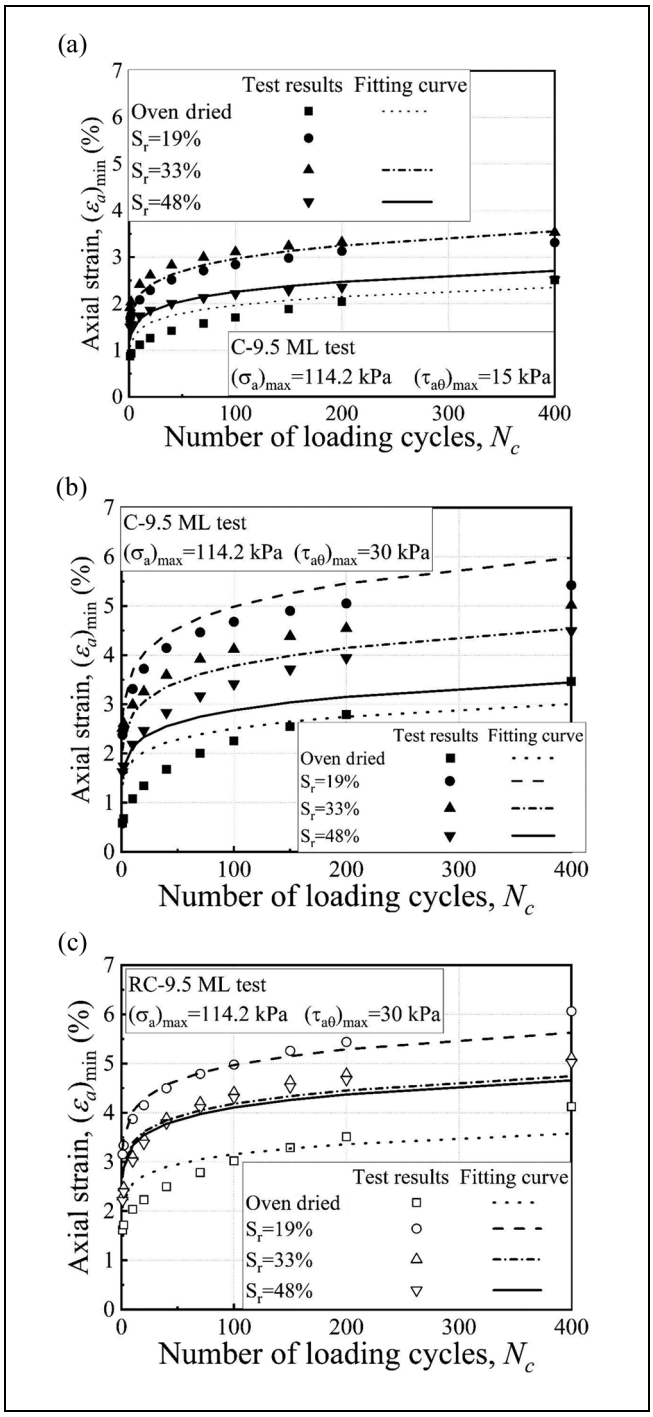

Figure 6. Estimation of the permanent strain of C-9.5 and RC-9.5 with fixed *A, B, C, D*, showing (*a*) C-9.5 in ML test ($[\tau_{a\theta}]$max = 15 kPa), (*b*) C-9.5 in ML test ($[\tau_{a\theta}]$max = 30 kPa), and (*c*) RC-9.5 in ML test.

z is depth within the base layer.

Figure 8 shows the predictive rut depth at 100,000 cycles through the modified UIUC model. The rut depth of oven-dried material is smallest and material with a 19% degree of saturation has the largest deformation

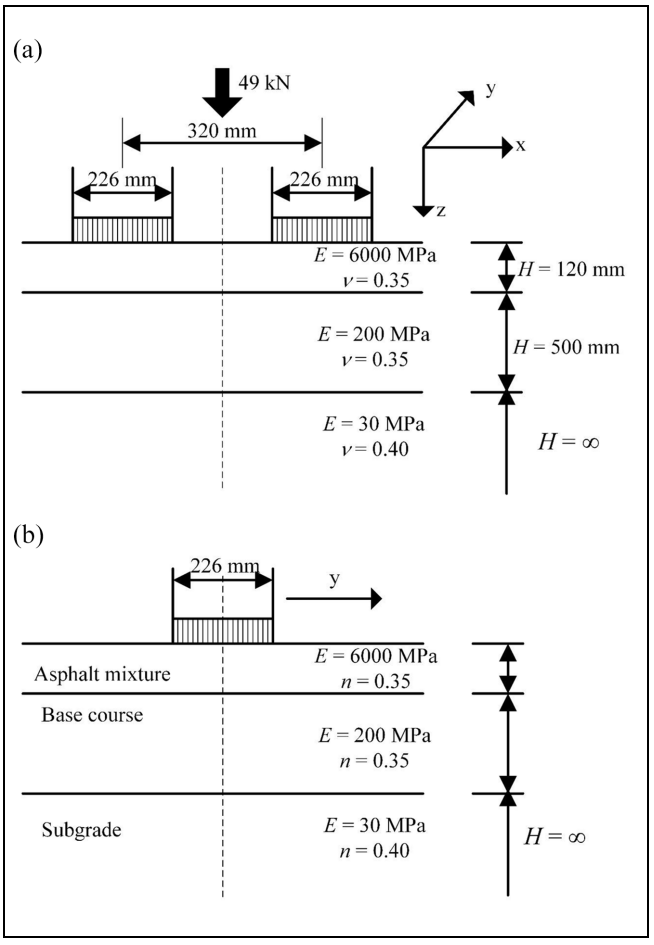

Figure 7. Model for stress analysis, showing (*a*) cross section and (*b*) longitudinal section.

regardless of the type of materials. In addition, the predictive rut depth through the UIUC model and MEPDG model are also shown in Figure 8. MEPDG gives the smallest rut depth, and the predictive rut depths of C-9.5 with different water contents are almost the same, which is not consistent with test results. Predictive rut depth through the UIUC model is much larger than that of MEPDG and varies with water content. However, it gives similar rut depth for two materials regardless of water content, which is also not consistent with test results. It is noted that the modified UIUC model gives much larger rut depth than other models. Moreover, predictive rut depth through the modified UIUC model varies with different water content and materials, which is consistent with test results. One reason for this difference is that modified UIUC considers the great effect of PSAR on permanent strain and this effect is ignored by other models. As discussed before, PSAR greatly improves the permanent strain accumulation. Moreover, the rut depths of RC-9.5 with 33% and 48% degree of saturation show little difference, though they have

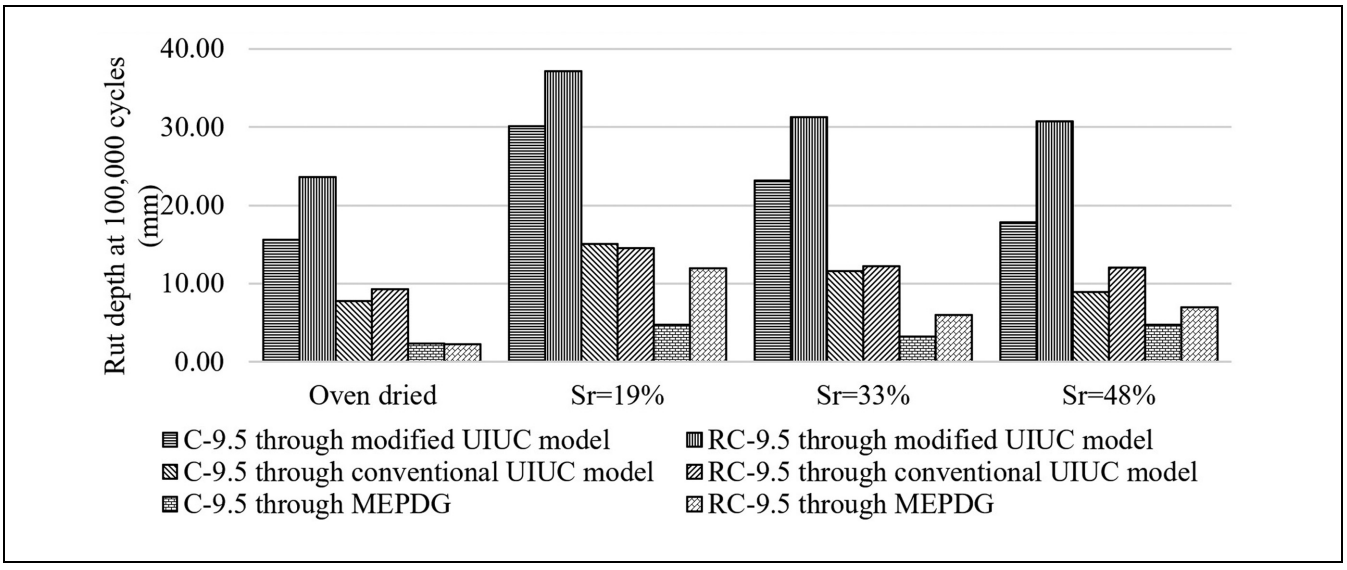

Figure 8. Computation of rut depth using modified UIUC model.

different estimated shear strength. This phenomenon implies a synergistic effect of change in water content and PSAR on permanent strain of unbound aggregate materials. In other words, the effect of PSAR on permanent strain accumulation may also be influenced by change in water content and this synergistic effect still needs further investigation.

Summary and Conclusions

This study modifies the UIUC model to evaluate the permanent deformation behavior of unbound aggregates. The following conclusions are obtained:

1. Shear strength has a more significant influence on permanent deformation of unbound aggregate materials than that of resilient properties.
2. PSAR greatly increases the permanent deformation behavior, and the newly added parameter, $(R_s)_{ave}$, could connect permanent deformation behavior with and without PSAR.
3. The modified UIUC model shows good applicability for prediction of permanent deformation of unbound aggregates with different water contents and stress states.
4. A simple framework is proposed to predict rut depth of base layers in flexible pavement structures based on the regression analysis results obtained from the modified UIUC model.

The modified UIUC model developed in this study needs further validation, as these findings are obtained through limited aggregate material types and have not been calibrated through comparing with actual rutting depth. Further and more comprehensive studies including more pavement materials and actual field performance to further validate these findings are recommended.

Acknowledgments

This research was supported in part by Grant-in-Aid for Scientific Research (C) (18560479) and (B) (20360206) from Japan Society for the Promotion of Science (JSPS) KAKENHI. The authors also acknowledge the support by China Scholarship Council. The constructive discussion with Prof. Erol Tutumluer is highly acknowledged by the authors.

Author Contributions

TI conceived of the presented idea and was in charge of overall direction and planning. TL analyzed the test data, performed the regression analysis, and wrote the manuscript with support from TI. BL performed the numerical simulations to implement the model.

References

1. ARA, Inc., *ERES Consultants Division. Guide for Mechanistic-Empirical Design of New and Rehabilitated Pavement Structures*. Final report, NCHRP Project 1-37A. Transportation Research Board of the National Academies, Washington, D.C., 2004.
2. Tseng, K. H., and R. L. Lytton. *Prediction of Permanent Deformation in Flexible Pavements Materials, Implication of Aggregates in the Design, Construction, and Performance of Flexible Pavements*. ASTM STP 1016. ASTM, West Conshohocken, Pa., 1989, pp. 154–172.

3. Saeed, A., J. W. Hall, and W. Barker. *NCHRP Report 453: Performance-Related Tests of Aggregates for Use in Unbound Pavement Layers*. TRB, National Research Council, Washington, D.C., 2001.
4. Korkiala-Tanttu, L. Verification of Rutting Calculation for Unbound Road Materials. *Proceedings of the Institution of Civil Engineers-Transport*, Vol. 162, No. 2, 2009, pp. 107–114.
5. Chow, L., D. Mishra, and E. Tutumluer. Framework for Development of an Improved Unbound Aggregate Base Rutting Model for Mechanistic-Empirical Pavement Design. *Transportation Research Record: Journal of the Transportation Research Board*, 2014. 2401: 11–21.
6. Miura, K., S. Miura, and S. Toki. Deformation Behavior of Anisotropic Dense Sand under Principal Stress Axis Rotation. *Journal of Soils and Foundations*, Vol. 26, No. 1, 1986, pp. 36–52.
7. Chan, F.W.K., and Brown, S.F. Significance of Principal Stress Rotation in Pavements. *Proc., 13th International Conference on Soil Mechanics and Foundation Engineering*, 1994, pp. 1823–1826.
8. Brown, S. F. Soil Mechanics in Pavement Engineering. *Geotechnique*, Vol. 46, No. 3, 1996, pp. 383–426.
9. Gräbe, P. J., and C. R. I. Clayton. Effects of Principal Stress Rotation on Permanent Deformation in Rail Track Foundations. *Journal of Geotechnical and Geoenvironmental Engineering*, Vol. 135, No. 4, 2009, pp. 555–565.
10. Ishikawa, T., S. Miura, and E. Sekine. Development and Performance Evaluation of Multi-Ring Shear Apparatus. *Proc., International Workshop on Geotechnical Aspects and Processed Material*, 2007, pp. 53–64.
11. Inam, A. *Performance Evaluation of Unsaturated Base Course Materials Subject to Repeated Traffic Loads*. Hokkaido University, 2012.
12. Monismith, C. L., N. Ogawa, and C. R. Freeme. Permanent Deformation Characteristics of Subgrade Soils Due to Repeated Loading. *Transportation Research Record: Journal of the Transportation Research Board*, 1975. 537: 1–17.
13. Chow, L. C., D. Mishra, and E. Tutumluer. *Aggregate Base Course Material Testing and Rutting Model Development*. Final Report, NCDOT Project 2013-18, FHWA/NC/2013-18. North Carolina Department of Transportation Research and Analysis Group, Raleigh, N.C., 2014.
14. AASHTO T307-99. *Standard Method of Test for Resilient Modulus of Subgrade Soils and Untreated Base/Subbase Materials*. AASHTO, Washington, D.C., 2003.
15. Ishikawa, T., E. Sekine, and S. Miura. Cyclic Deformation of Granular Material Subjected to Moving-Wheel Loads. *Canadian Geotechnical Journal*, Vol. 48, No. 5, 2011, pp. 691–703.
16. Inam, A., T. Ishikawa, and S. Miura. Effect of Principal Stress Axis Rotation on Cyclic Plastic Deformation Characteristics of Unsaturated Base Course Material. *Soils and Foundations*, Vol. 52, No. 3, 2012, pp. 465–480.
17. Maina, J. W., and K. Matsui. Developing Software for Elastic Analysis of Pavement Structure Responses to Vertical and Horizontal Surface Loadings. *Transportation Research Record: Journal of the Transportation Research Board*, 2004. 1896: 107–118.
18. Duncan, J. M., and C. Y. Chang. Nonlinear Analysis of Stress and Strain in Soils. *Journal of the Soil Mechanics and Foundations Division*, Vol. 96, 1970, pp. 1629–1653.
19. Ishikawa, T., S. Miura, and E. Sekine. Simple Plastic Deformation Analysis of Ballasted Track Under Repeated Moving-Wheel Loads by Cumulative Damage Model. *Transportation Geotechnics*, Vol. 1, No. 4, 2014, pp. 157–170.
20. *Pavement Design Manual*. Japan Road Association, Tokyo, 2006. (in Japanese)

The Standing Committee on Engineering Behavior of Unsaturated Geomaterials (AFP60) peer-reviewed this paper (19-04431).